 CMC, vol.35, no.3, pp.229-254, 2013

Multiscale Fatigue Life Prediction for Composite Panels

Brett A. Bednarcyk[1], Phillip W. Yarrington[2], Steven M. Arnold[3]

Abstract: Fatigue life prediction capabilities have been incorporated into the HyperSizer Composite Analysis and Structural Sizing Software. The fatigue damage model is introduced at the fiber/matrix constituent scale through HyperSizer's coupling with NASA's MAC/GMC micromechanics software. This enables prediction of the micro scale damage progression throughout stiffened and sandwich panels as a function of cycles leading ultimately to simulated panel failure. The fatigue model implementation uses a cycle jumping technique such that, rather than applying a specified number of additional cycles, a specified local damage increment is specified and the number of additional cycles to reach this damage increment is calculated. In this way, the effect of stress redistribution due to damage-induced stiffness change is captured, but the fatigue simulations remain computationally efficient. The model is compared to experimental fatigue life data for two composite facesheet/foam core sandwich panels, demonstrating very good agreement.

1 Introduction

Composite sandwich and stiffened panels are common acreage structural concepts for efficient modern aircraft and spacecraft design. Polymer matrix composites offer excellent material properties per unit weight and, when arranged intelligently to form a panel, full advantage of their properties can be taken to provide a structure with optimal strength, stiffness, and stability. However, care must be taken in the panel design to consider the appropriate local loads as well as the full range of failure modes that may be encountered. The HyperSizer Composite Analysis and Structural Sizing Software [Collier Research Corp (2013)] offers a convenient means to address this problem. As shown in Figure 1, this software relies on a structural scale finite element model to determine element loads for each load case. Panels are defined as groups of elements, and, to arrive at panel design-to loads, the software statistically processes the element loads for each load case. These loads

[1] NASA Glenn Research Center, Cleveland, OH, 44135
[2] Collier Research Corp., Newport News, VA, 23606
[3] NASA Glenn Research Center, Cleveland, OH, 44135

are then localized to determine laminate and ply level stresses and strains. A multitude of static strength and stability failure criteria are checked for the panel and all its subcomponents (e.g., facesheets, core, stiffener web) to find the lightest panel (in terms of materials and geometry) for which no failure criteria are exceeded. The software then writes new material definitions for all the panels to the structural finite element model, which is re-executed to determine a new static solution based on the updated design. This process is repeated iteratively until a converged design is reached.

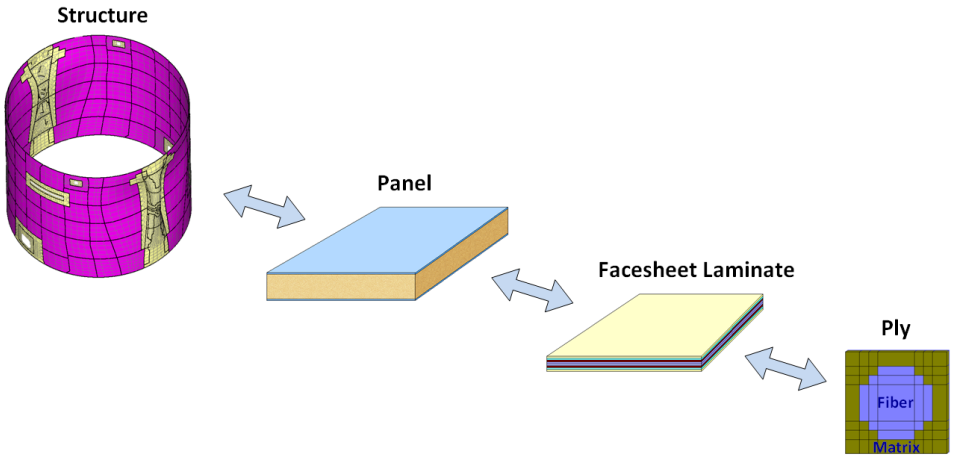

Figure 1: Schematic of the HyperMAC multiscale design and analysis software that localizes and homogenizes across the scales of the structure, panel, panel subcomponent, and ply, to the composite constituents.

Recently, the standard HyperSizer design and analysis procedure, which localizes to the level of the ply, has been enhanced through coupling with NASA's Micromechanics Analysis Code with Generalized Method of Cells (MAC/GMC) software [Bednarcyk and Arnold (2002)] to enable localization to the fiber and matrix constituent scale (Figure 1) using the Generalized Method of Cells (GMC) and High Fidelity Generalized Method of Cells (HFGMC) micromechanics theories [Aboudi, Arnold and Bednarcyk (2013)]. This coupled software, called HyperMAC [Bednarcyk, Yarrington, Collier and Arnold (2006); Bednarcyk and Arnold (2010)], can now predict the properties of composite materials for use in the standard HyperSizer design process. Furthermore, progressive failure of the fiber and matrix constituents can be simulated, and the effects of this local damage on the higher scale behavior can be predicted. Static failure predictions for composite panels using the HyperMAC software were presented in refs. [Bednarcyk, Yarrington, Collier and

Arnold (2006); Bednarcyk and Arnold (2010)]. Now, the HyperMAC capability has been further extended to enable cyclic fatigue life predictions for composite stiffened and sandwich panels. The addition of fatigue calculations represents an important additional failure mechanism that was not previously considered by HyperSizer. The presented approach captures the physics of panel fatigue damage and failure at the constituent scale (where damage actually occurs) based on the micro scale stress-strain history throughout the panel. By handling fatigue damage at the micro scale, an isotropic fatigue model can be employed, whereas at the ply level, a more complex anisotropic approach would be required. Additionally, a ply level model would need re-characterization for every variation in ply fiber volume fraction, whereas the HyperMAC multiscale model can prediction the influence of fiber volume fraction and other microstructural features.

As discussed by Dong and Atluri [Dong and Atluri (2013)] and Aboudi et al. [Aboudi, Arnold and Bednarcyk (2013)], computational efficiency is a key consideration for micromechanics modeling of composites as it necessitates additional computational effort compared to ply level approaches. This is particularly true in multiscale analysis and in design and sizing, which typically require many repeated analyses. Use of an ultra-efficient micromechanics approach, like the GMC used herein, can provide a good approximation of the local constituent fields, but at a fraction of the computational cost of the standard unit cell based finite element approach or multiscale finite element approaches (e.g., [Feyel (1999); Chrupalla, Kreikemeier, Berg, Kärger, Dorielle, Ludwig, Jansen, Rolfes and Kling (2012)]).

Sharma et al. [Sharma, Gibson and Ayorinde (2006)] provided a review of composite sandwich panel fatigue modeling wherein they broadly categorized the work into four main areas: (i) the basic S-N approach [Kanny and Mahfuz (2005)-Zenkert and Burman (2011)], (ii) the strength degradation approach [Dai and Hahn (2004)], (iii) the stiffness reduction approach [El Mahi, Farooq, Sahraoui and Bezazi (2004); Abbadi, Azari, Belouettar, Gilgert and Freres (2010)], and (iv) cumulative damage modeling (to deal with the effects of variable loading). Sharma et al. [Sharma, Gibson and Ayorinde (2006)] also point to the need to move away from high volume, higher scale fatigue testing of sandwich panels in favor of validated physics-based predictive models. The present work addresses this need as it predicts the panel fatigue life based solely on the panel geometry and static strength and fatigue properties of the panel constituent materials. The methodology also represents a synergistic combination of three of the approaches identified by Sharma et al. [Sharma, Gibson and Ayorinde (2006)]. The basic S-N approach is used for the sandwich panel core, whereas the stiffness reduction approach is used for the constituent materials within the facesheet plies. At this constituent micro scale, cumulative damage modeling is also employed such that a certain amount of damage accumu-

lates in the composite constituents based on the number of cycles at a given local cyclic stress range. This local stress range, in general, varies as the panel damages in a progressive manner and the stresses redistribute.

Additional recent relevant work on fatigue modeling has been published by Xiang and Liu [Xiang and Liu (2010), Xiang and Liu (2011)], who addressed the probabilistic nature of fatigue loading, and Jen and Chang [Jen and Chang (2008)-Jen and Chang (2009b)] and Camata and Shing [Camata and Shing (2010)], who found that fatigue-induced delamination between the core and facesheets is an important damage mechanism in fatigue life prediction for honeycomb sandwich panels. The present work is solely deterministic and, at this time, the approach does not consider delamination, which was not observed in the foam core sandwich panels modeled herein. However, cyclic debonding and delamination methods have recently been developed and implemented within the GMC micromechanics framework by Naghipour et al. [Naghipour, Pineda and Arnold (2013)].

The remainder of this paper outlines the theoretical underpinnings of the fatigue damage simulation capability, which operates at the fiber/matrix constituent scale, along with its implementation into HyperMAC. The capability is validated via comparison to fatigue data (S-N curves) derived from tests on two types of E-glass/vinylester foam core sandwich beams that have recently appeared in the literature [Zenkert and Burman (2011)].

2 Composite Static Deformation, Damage, and Failure

The composite laminates considered herein, which form the facesheets of the foam core sandwich beams considered below, are quasi-isotropic E-glass/vinylester manufactured via VARTM. The reinforcement is a DBLT-850-E10 quadriaxial noncrimp E-glass fabric [Devold AMT (2011)], while the resin is Reichhold DION 9500 vinylester [Reichhold, Inc. (2011)]. Based on a per ply areal mass of 200 g/m^2 [Zenkert and Burman (2011)], an infused ply thickness of 0.1875 mm [Zenkert and Burman (2011)], and an E-glass density of 2550 kg/m^2, the fiber volume fraction of the laminate was estimated to be 42%.

The E-glass/vinylester composite laminate was modeled within HyperSizer using the HyperMAC micromechanics capability. This capability enables the ply level materials to be simulated using NASA's Micromechanics Analysis Code with Generalized Method of Cells (MAC/GMC) [Bednarcyk and Arnold (2002)], which relies on the Generalized Method of Cells (GMC) [Aboudi (2004)] micromechanics theory. The GMC repeating unit cell used to represent the E-glass/vinylester composite is shown in Figure 2. In GMC, the subvolumes, or subcells, contain constituent materials whose properties are needed as input. The E-glass fiber and

vinylester resin were both taken to be isotropic with elastic properties given in Table 1. Loading is applied incrementally, and a given subcell is predicted to fail when its local stress or strain field exceeds a specified failure criterion. The subcell is then assigned very low stiffness components (0.0001 times the original stiffness components), which, when homogenized with the other subcell contributions, causes the composite effective stiffness to decrease. If the composite represents a ply in a laminate, as it does in the present case, the stiffness of the laminate is decreased each time a subcell fails as the incremental loading on the laminate continues. Likewise, if the laminate is part of a stiffened or sandwich panel, as the subcells fail, the panel stiffness will decrease. Final failure can then be predicted using a panel level failure criterion. Herein, this criterion examines the change in the value of the trace of the inverse of the panel ABD matrix, a measure of the panel's compliance. When this value increases by a factor of 10, the panel is considered to be failed [Bednarcyk, Yarrington, Collier and Arnold (2006)]. Note that this is intended to represent acreage panels. Accounting for discontinuities such as ply drops, penetrations, and joints requires additional stress solutions, some of which are provided in HyperSizer [Collier Research Corp. (2013)].

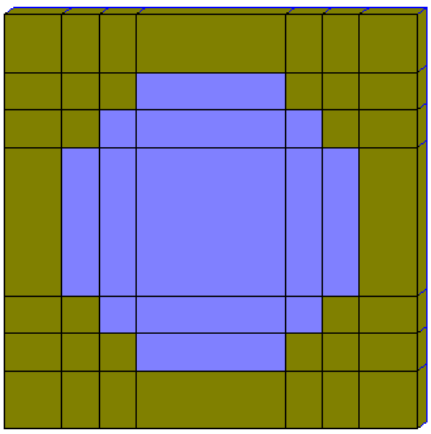

Figure 2: GMC repeating unit cell used to represent the E-glass/vinyl ester ply level composite material.

A progressive failure analysis of the tensile response of the $[0/45/90/-45]_s$ 42% volume fraction E-glass/vinylester solid laminate (described in ref. [Zenkert and Burman (2011)]) was performed using HyperMAC. The simulation modeled the laminate using the classical lamination theory capabilities within HyperSizer, with the results shown in Figure 3. Damage, in the form of subcell failures, initiates

Table 1: . Composite constituent elastic properties

	E (GPa)	ν	**Tensile Strength (MPa)**
E-glass [27]	80	0.2	2150
Vinylester [25]	3.1	0.3	70

at 112 MPa. Because the simulation was performed in strain control (i.e., the axial midplane strain component on laminate was monotonically increased, while all force and moment resultants were kept at zero), each loss of stiffness results in a decrease in stress, followed by continued loading with a reduced slope. Were the complete experimental stress-strain curve provided, one would not expect to observe such obvious stress decreases. Rather, the experimental stiffness decrease would be more gradual than the simulation, which considers the entire specimen as a single point in the plane of the laminate. In addition, because all nonlinearity in the simulation is associated with damage in the form of local stiffness decreases, each loading portion of the predicted stress-strain curve follows a line that passes through the origin. Unloading data, were it provided, could provide an assessment of the accuracy of modeling all nonlinearity as stiffness reduction. Several failure events occur within the laminate before a large event that causes a significant decrease in stress and stiffness signals failure of the panel. The predicted laminate tensile strength is 306 MPa, compared to a measured value of 310 MPa [Zenkert and Burman (2011)]. It should be noted that in this and subsequent simulations, the max stress, max strain, and Tsai-Hill failure criteria were all active for each subcell. If any of these criteria are exceeded, subcell failure is activated. The material failure strains were assumed to be the tensile strength (Table 1) divided by Young's modulus.

3 Composite Fatigue

Like the static failure and damage methodology employed within HyperMAC, the cyclic fatigue damage capability considers the fiber/matrix constituent scale by applying damage to the subcells based on the stress and strain history at this scale. Thus, when loading is applied to a panel, the loads are localized to the laminate, ply, and subcell scale to obtain these histories. The fatigue damage model implemented within HyperMAC is a transversely isotropic extension of the NonLinear Cumulative Damage Rule (NLCDR) developed at ONERA (Office Nationale d'Etudes et de Recherches Aerospatiales) for isotropic materials The development of this model was presented by Arnold and Kruch [Arnold and Kruch (1991); Arnold and Kruch (1994)] and its implementation within GMC was described by Wilt et al.

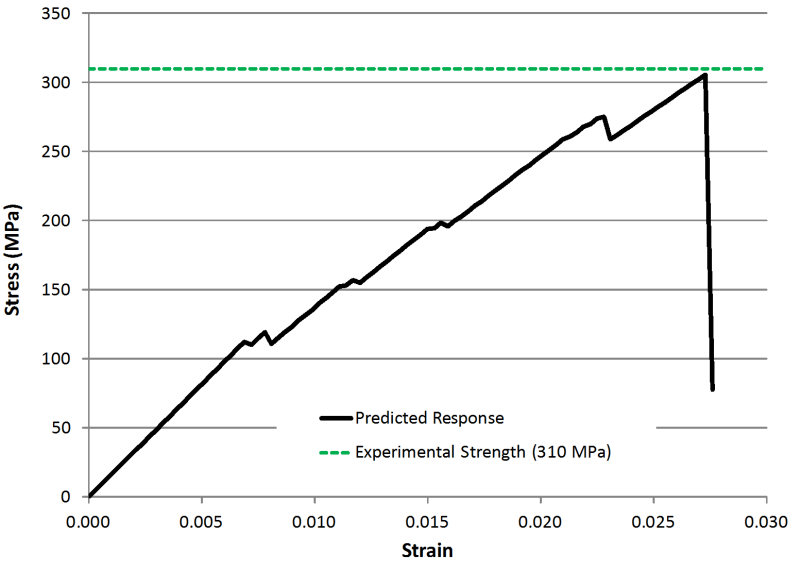

Figure 3: . HyperMAC prediction of the tensile response of a $[0/45/90/-45]_s$ 42% volume fraction E-glass/vinylester composite laminate.

[Wilt, Arnold and Saleeb (1997)]. A damage variable, D, evolves with number of cycles, and, for a given damage level, the stiffness of a subcell is degraded by (1 – D), where D = 0 corresponds to a pristine subcell and as D approaches 1, the subcell approaches a failed state. As with static failure, the actual subcell stiffness reduction is capped at a factor of 0.0001 (D = 0.9999).

The evolution of damage is governed by,

$$\int_{D_{k-1}}^{D_k} dD = \int_0^N \left[1-(1-D)^{\beta+1}\right]^{\alpha} \left[\frac{\hat{F}_m}{1-D}\right]^{\beta} dN \tag{1}$$

where N is the number of cycles at the current stress state (σ_k), D_k and D_{k-1} are the amount of damage after the current and previous damage increments, respectively, $\beta$is a material parameter, and α is a function of the current stress state,

$$\alpha = 1 - \hat{a}\frac{\sigma_{fl}}{\sigma_u}\frac{\langle \Phi_{fl} \rangle}{\langle \Phi_u \rangle} \tag{2}$$

$\hat{a}$ is a material parameter, and $\langle\rangle$ are Macauley brackets. σ_{fl} and σ_u are the uniaxial fatigue limit and ultimate strength material properties, respectively, and Φ_{fl} and Φ_u

are the fatigue limit and static fracture surfaces, respectively,

$$\Phi_{fl} = \frac{1}{2}\frac{\max}{t_0}\frac{\max}{t}F_{(\sigma_{fl})}\left[\sigma_{ij}(t) - \sigma_{ij}(t_0)\right] - 1 \tag{3}$$

$$\Phi_u = 1 - \frac{\max}{t}F_{(\sigma_u)}\left[\sigma_{ij}(t)\right] \tag{4}$$

The operator $\frac{\max}{t}$ indicates that the maximum value of the expression to the right up to time t of the current load cycle should be taken. The normalized stress amplitude is defined as,

$$\hat{F}_m = \frac{1}{2}\frac{\max}{t}\frac{\max}{t_0}F_{(M)}\left[\sigma_{ij}(t) - \sigma_{ij}(t_0)\right] \tag{5}$$

When $\langle\Phi_u\rangle = 0$, static fracture (complete local failure) is indicated, thus α cannot be defined. $\langle\Phi_{fl}\rangle = 0$ indicates that the current stress state is below the fatigue limit and α is set to one. This then represents a special case when integrating eq. (1) that will be considered separately. The t_0 and t terms in eqs. (3) – (5) are the time at the beginning of the current load cycle and the current time during the current load cycle, respectively.

The general form for the terms $F_{(\sigma_{fl})}$, $F_{(\sigma_u)}$, and $F_{(M)}$ can be expressed as,

$$F_{()} = \sqrt{\frac{1}{()_L^2}\left[\left(4\omega_{()}^2 - 1\right)I_1 + \frac{4\omega_{()}^2 - 1}{\eta_{()}^2}I_2 + \frac{9}{4}I_3\right]} \tag{6}$$

where,

$$\begin{aligned} I_1 &= \tfrac{1}{2}S_{ij}S_{ij} - d_i d_j S_{jk}S_{ki} + \tfrac{1}{4}\left(d_i d_j S_{ij}\right)^2 \\ I_2 &= d_i d_j S_{jk}S_{ki} - \left(d_i d_j S_{ij}\right)^2 \\ I_3 &= \left(d_i d_j S_{ij}\right)^2 \end{aligned} \tag{7}$$

The current deviatoric stress components are $S_{ij} = \sigma_{ij} - \frac{1}{3}\sigma_{mm}\delta_{ij}$, and d_i are the components of the vector defining the preferred direction in a transversely isotropic material. $\omega_{()}$ and $\eta_{()}$ represent the ratios of longitudinal to transverse normal and shear stresses, respectively, for a transversely isotropic material and are equal to one for an isotropic material. Note that, in calculating $F_{(M)}$ with eq. (6), the value of M, a material constant, is required. The L subscript in eq. (6) indicates the longitudinal direction in a transversely isotropic material.

For the case in which the current local stress state, σ_k, is above the initial fatigue limit, the number of cycles, N, required to damage a subcell from a level of D_{k-1}

to D_k is obtained by integrating eq. (1) and is given by,

$$N = \frac{\left\{ \left[1-(1-D_k)^{\beta-1} \right]^{1-\alpha} - \left[1-(1-D_{k-1})^{\beta+1} \right]^{1-\alpha} \right\}}{\hat{F}_m^{\beta} (1-\alpha)(\beta+1)} \tag{8}$$

When the local stress level is below the fatigue limit, $\alpha = 1$, integration of eq. (1) yields,

$$N = \frac{\log \left[1-(1-D_k)^{\beta-1} \right] - \log \left[1-(1-D_{k-1})^{\beta+1} \right]}{\hat{F}_m^{\beta} (\beta+1)} \tag{9}$$

Equations (8) and (9) can also be solved for D_k in order to determine the current amount of damage developed for a given number of cycles and previous state of damage, D_{k-1}. Further, to determine the remaining cycles to failure for a given previous state of damage, D_k can be set equal to one in eqs. (8) and (9).

The implementation of this fatigue model within HyperMAC enables cycle jumping (i.e., not explicitly modeling every fatigue cycle for reasons of computational efficiency) and stress redistribution by using a specified damage increment. HyperMAC applies a single loading cycle to the panel, determines the stress-strain history in each subcell of every ply, and then calculates the number of additional cycles required to damage each subcell by an additional amount equal to the specified damage increment using eqs. (8) and (9). The controlling subcell throughout all plies and all laminates within the panel is found as the subcell with the smallest required number of additional cycles. This number of cycles is then applied to the entire panel, and the new damage level in each subcell is calculated. Then, another single loading cycle is applied to the panel, and a new stress-strain history for each subcell is determined. These subcell stress-strain histories will, in general, be different than the histories obtained from the previously applied loading cycle due to the presence of additional damage and the associated stress redistribution. This process is repeated, and the total number of cycles on the panel is summed, until complete failure of the panel is predicted (again, using the trace of the inverse of the ABD matrix criterion described previously). If a static failure of a subcell is detected in response to application of the load cycle, the total number of cycles is incremented by 1, and the load cycle is applied again to capture the redistribution associated with the failure event.

The HyperMAC fatigue implementation is based on constituent material fatigue properties that can be determined from one or more constituent S-N curves. Assuming that the ultimate strength is known as a static failure property, the required fatigue material parameters for an isotropic constituent are: β, $\hat{a}$, σ_{fl}, and M. However, in the present application to foam sandwich beam tests [Zenkert and Burman

(2011)], constituent fatigue data were not provided. This reference did, however, provide facesheet quasi-isotropic laminate tensile fatigue data, which were used to back out the vinylester resin fatigue parameters. The tests and simulations both used a value of $R = \sigma_{min}/\sigma_{max}$ = 0.1. It was assumed that the E-glass fiber is not subject to fatigue damage, but that it could fail statically during the fatigue simulations. A damage increment of 0.2 was used in the simulations.

The characterization of the vinylester fatigue parameters to reproduce the quasi-isotropic laminate tensile fatigue data using HyperMAC is shown in Figure 4. Clearly, the calibrated model does an excellent job of reproducing the laminate fatigue S-N curve. Also plotted is the Basquin's Law representation of the data as presented by Zenkert and Burman [Zenkert and Burman (2011)],

$$\sigma_{\max} = BN^{-1/\gamma} \tag{10}$$

where the parameters for the homogenized laminate are: B = 498 MPa and γ = 7.88. The HyperMAC multiscale fatigue model correlates significantly better with the experimental data than does the Basquin's Law characterization, which is linear on the log-log plot. The vinylester fatigue parameters resulting from the correlation shown in Figure 4 are given in Table 2, and the fatigue S-N curve that these parameters represent for the vinylester resin is shown in Figure 5 (again, for R = 0.1).

Table 2: Characterized neat vinylester resin fatigue model parameters.

parameter	**value**	**parameter**	**value**
ω_u	1.0	β	4.25
ω_{fl}	1.0	$\hat{a}$	0.3
ω_m	1.0	σ_{fl}	7. MPa
η_u	1.0	M	135 MPa
η_{fl}	1.0	σ_u	70. MPa
η_m	1.0		

4 Foam Core Beam Fatigue

Two types of foam core sandwich beams were tested by Zenkert and Burman [Zenkert and Burman (2011)], one with a Divinycell H100 PVC foam core [DIAB AB (2011)] and one with a Rohacell WF51 PMI foam core [Evonik Industries (2011)]. The elastic properties of these materials are given in Table 3. Zenkert and Burman [Zenkert and Burman (2011)] provided shear fatigue data for these two

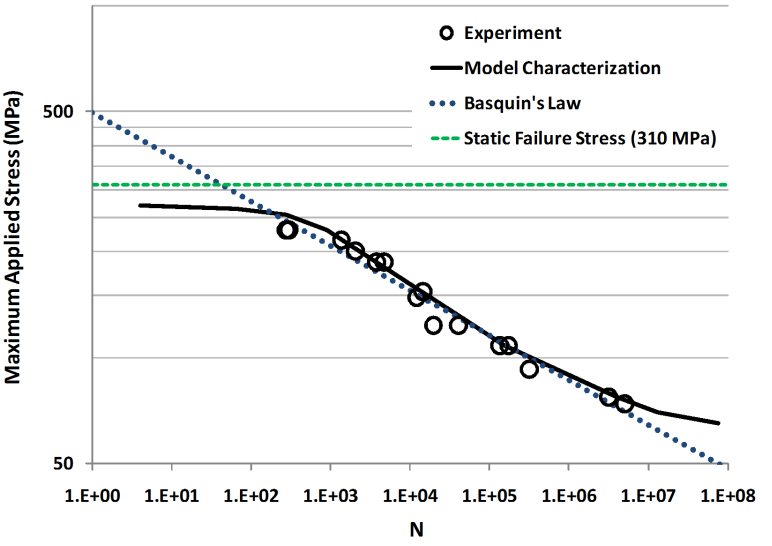

Figure 4: Correlation of calibrated model with experimental tensile fatigue data [Zenkert and Burman (2011)] for a $[0/45/90/-45]_s$ 42% volume fraction E-glass/vinylester composite ($R = 0.1$). The Basquin's Law parameters (see Eq. (10)) are: B = 498 MPa and $\gamma = 7.88$.

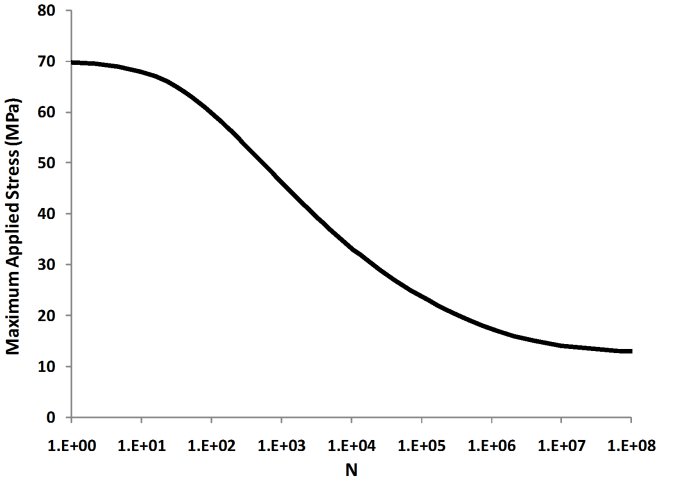

Figure 5: Characterized neat vinylester resin fatigue S-N curve for $R = 0.1$.

types of foam, as shown in Figure 6, based on four point bend tests. Also plotted are the Basquin's Law fits to these data, where the parameters are: for Divinycell H100 B = 2.34 MPa, γ = 12.08; for Rohacell WF51 B = 0.858 MPa, γ = 19.8. These Basquin's Law curves are cut off at the shear yield stress for each foam, as given in Table 3.

Table 3: Foam core material properties [Zenkert and Burman (2011)].

Property	Divinycell H100	Rohacell WF51
E (MPa)	126	75
G (MPa)	40	27
τ_{yield} **(MPa)**	1.13	0.66

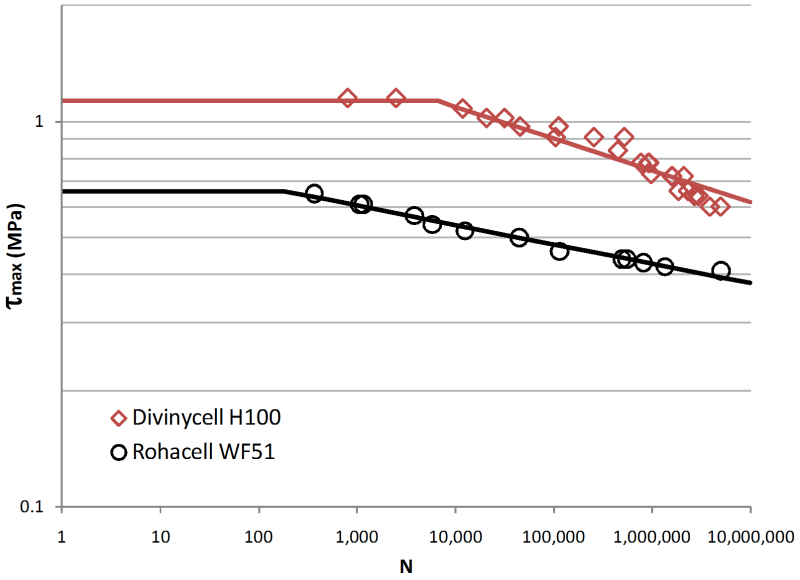

Figure 6: Shear fatigue test data ($R = 0.1$) for Divinycell H100 and Rohacell WF51 foam materials along with Basquin's Law curves. The Basquin's Law parameters are: for Divinycell H100 B = 2.34 MPa, γ = 12.08; for Rohacell WF51 B = 0.858 MPa, γ = 19.8.

The foam core sandwich beams constructed and tested by Zenkert and Burman [Zenkert and Burman (2011)] consisted of a thicker top facesheet and a thinner

bottom facesheet, as shown in Figure 7. This was motivated by the desire to have facesheet damage and failure occur only in tension in the bottom facesheet when the beams were tested in four point bend loading as shown in Figure 8 (the top facesheet is in compression). The test beam dimensions are given in Table 4, where, it should be noted that the Divinycell H100 core beam facesheet thicknesses are correct [Zenkert (2011)], despite the fact that the nominal dimensions (t_1 = 3.0 mm, t_2 = 1.5 mm) were listed in ref. [Zenkert and Burman (2011)]. The four point bend tests were conducted using a value of $R = 0.1$.

The two types of foam core beams were modeled in HyperMAC using the software's sandwich panel design/analysis capability. This enables specification of the ply materials, lay ups, core material, and dimensions. The ply materials were represented using the MAC/GMC coupling with the repeating unit cell shown in Figure 2. The E-glass and vinylester constituent material properties given in Table 1 and Table 2 were employed and, similar to the static failure simulation for the facesheets presented above, the max stress, max strain, and Tsai-Hill static failure criteria were active for the constituents. As in the laminate fatigue characterization results presented above, only the vinylester matrix constituent was subject to fatigue damage. Further, since the thicker top facesheet remains in compression in the tests while the fatigue model was characterized for facesheet tension only, damage and failure was not permitted in the thicker top facesheet in the simulations.

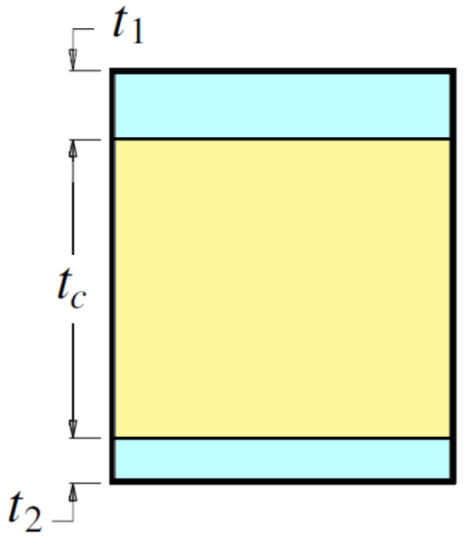

Figure 7: Foam core sandwich beam cross-section dimensions.

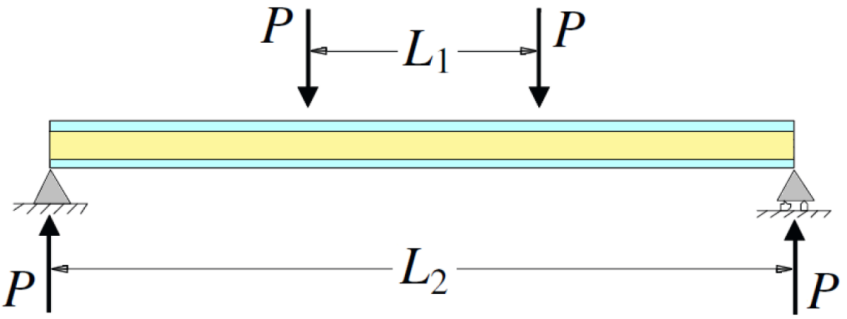

Figure 8: Foam core sandwich beam four point bend specimen dimensions.

Table 4: Foam core beam dimensions [13, 33].

	Divinycell H100 Core Beam	**Rohacell WF51 Core Beam**
Top Face	4 layers DBLT-850-E10 quadriaxial non-crimp E-glass fabric (16 plies symmetric)	4 layers DBLT-850-E10 quadriaxial non-crimp E-glass fabric (16 plies symmetric)
Bottom Face	2 layers DBLT-850-E10 quadriaxial non-crimp E-glass fabric (8 plies symmetric)	2 layers DBLT-850-E10 quadriaxial non-crimp E-glass fabric (8 plies symmetric)
t_c (mm)	50	50
t_1 (mm)	2.8	3.0
t_2 (mm)	1.4	1.5
L_1 (mm)	80	175
L_2 (mm)	500	1000

The foam core material was considered to be homogeneous and its fatigue behavior was modeled using the Basquin's Law relation, eq. (10), as plotted in Figure 6. This relation was implemented by lowering the shear allowable of the foam material in HyperMAC as a function of cycles; no core shear stiffness reduction was modeled. The Simplified Shear Solution [Bednarcyk, Aboudi and Yarrington (2007)] available within HyperSizer was used to calculate the through-thickness shear stress distribution in the core from the panel level through-thickness shear load. This solution results in a more realistic piece-wise parabolic through-thickness shear distribution rather than a constant core through-thickness shear value, as predicted by

simpler equations. The core shear stress could then be compared to the allowable (which changes as a function of number of cycles) to predict core failure, which was considered to represent panel failure.

The panel level loading in HyperMAC was applied to simulate the maximum load condition that occurs in the four point bend specimen according to beam theory at the locations directly below the applied load points (see Figure 8). That is, a moment equal to P $(L_2 - L_1)/2$ was applied (equal to the moment between the applied load locations), along with a through-thickness shear load equal to P (equal to the shear load between the end of the beam and the applied load locations). The simulations thus represent a single location along the four point bend specimen. As in the laminate simulations above, a damage increment of 0.2 was used. Further, as suggested in ref. [Zenkert and Burman (2011)], core failure was predicted using the provided core shear yield stress (see Table 3). The average calculated core shear stress was compared to this yield stress, which was reduced with number of cycles according to Basquin's Law (see Figure 6). The beam was considered to fail either by the standard HyperMAC panel failure criterion based on the inverse of the ABD matrix, or when the core failed (which ever occurred first). Note that the HyperSizer sandwich panel and beam method neglects the contribution of the core material to the panel axial stiffness. However, the core stiffness is used in calculating the through-thickness shear stress distribution [34].

Figure 9 compares the HyperMAC predictions with the experimental data provided by Zenkert and Burman [Zenkert and Burman (2011)] for the H100 foam core beam loaded in four point bending. Both the experimental and model data show a transition from a core shear failure mechanism to a facesheet tensile failure mechanism. In the experimental data, this transition occurred between 6309 cycles and 8767 cycles. In the model predictions, this transition happened at 7791 cycles. At slightly higher load levels (lower number of cycles) the beam failure mode transitions to static failure of the core (P_{max} = 58.9 N/mm). The agreement between the model predictions and experiment is excellent.

Figure 10 compares the HyperMAC model predictions for the H100 foam core beam with Basquin's Law predictions. For the Basquin's Law predictions, the facesheet stress is calculated as,

$$\sigma = \frac{M}{t_2\, d} = \frac{P\,(L_2 - L_1)}{2\, t_2\, d} \tag{11}$$

where M is the moment between the load application locations, and $d = t_c + t_1/2 + t_2/2$ is the distance between the facesheet centroids. P_{max} can then be calculated for a given number of cycles by substituting eq. (10) into eq. (11) and solving for P. For the foam core Basquin's Law calculation, the shear load, equal to P, is divided

by d to arrive at the average core shear stress. A similar substitution of Basquin's Law then allows the calculation of P_{max} as a function of number of cycles. Figure 10 shows that, for number of cycles greater than approximately 5000, Basquin's Law predicts a lower failure load for the facesheet compared to core, indicating that facesheet failure should control in the region of the figure. This corresponds to the experimental observation as shown in Figure 9. The Baquin's Law curves for the facesheet reach the core static shear strength before they intersect each other, but they are nearly converged at these points. The Basquin's Law core prediction is very close to the HyperMAC core prediction. For the facesheet, the Basquin's Law prediction is by definition linear (on this log-log plot), and thus there is some deviation from the HyperMAC prediction, which is nonlinear.

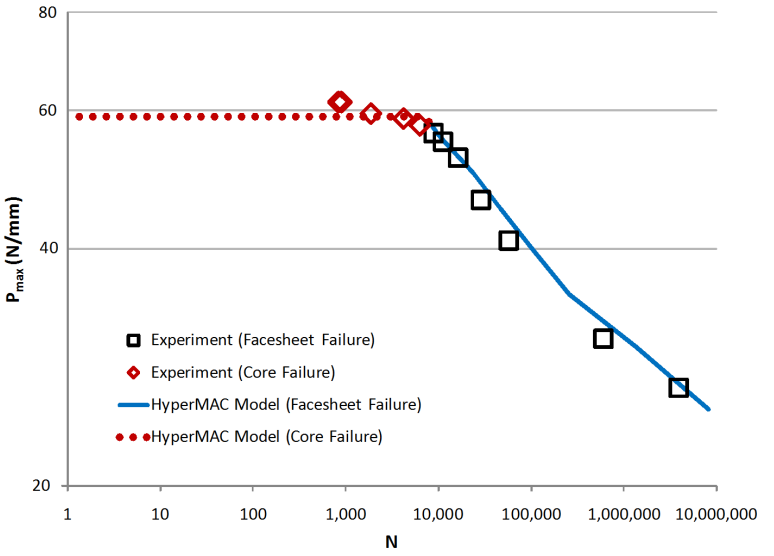

Figure 9: HyperMAC prediction of the fatigue life of the H100 foam core beam tested in four point bending, along with experimental data [Zenkert and Burman (2011)].

A final curve plotted in Figure 10 is the core failure predicted by HyperMAC if, instead of the average core shear stress, the maximum core shear stress is used to predict failure. This may be thought of more as a prediction of damage initiation in the core rather than complete core failure. As expected, at higher loads (lower number of cycles) this would result in a lower predicted P_{max} value compared to when the average core shear stress is used. Interestingly, when the beam transitions to facesheet failure at a higher number of cycles, the core maximum stress predic-

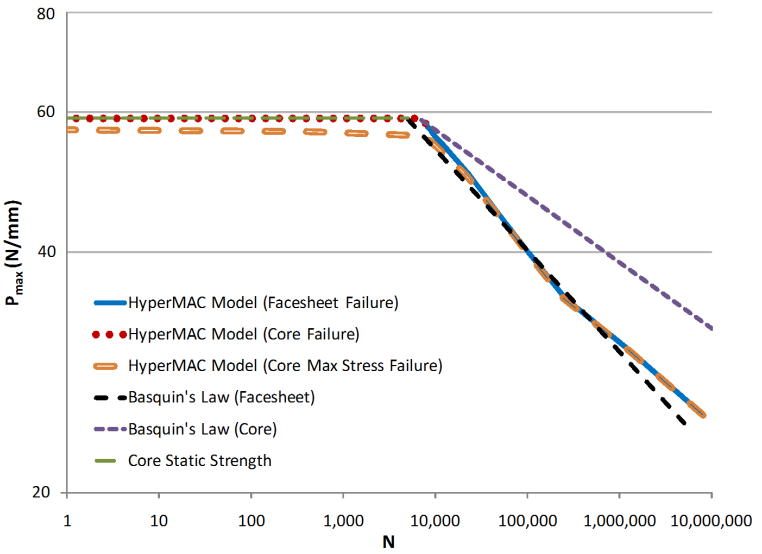

Figure 10: HyperMAC prediction of the fatigue life of the H100 foam core beam tested in four point bending, compared with Basquin's Law predictions.

tion begins to track closely with the facesheet failure prediction. This is because, at a given load level, as the bottom facesheet begins to accumulate damage, it softens. The shear stress in the bottom facesheet decreases, leading to the development of a gradient of shear stress through the thickness of the core where it was previously nearly uniform. The average shear stress in the core, however, is relatively unaffected. This is shown in Figure 11, where an example of the through-thickness shear stress distribution [Bednarcyk, Aboudi and Yarrington (2007)], as a function of facesheet damage, is plotted (albeit for the WF51 beam). In the pristine beam, the shear stress rises rapidly from zero in the facesheets but exhibits only slight variation from the core average in the core. Both the core average shear stress and the core maximum shear stress are well below the core static shear strength (0.66 MPa in this case of the WF51 core). Note that the shear stress distribution is parabolic in each ply and the core, and it is continuous at the interfaces. After 27,746 cycles, the bottom facesheet has been damaged, and, due to their reduced stiffness, the through-thickness shear stress cannot rise as rapidly in the damaged plies. As a result, the shear stress at the interface between the bottom facesheet and the core is significantly lower than in the pristine beam. Further, because the through-thickness shear stress distribution must still integrate to give the applied through-thickness shear load (which has not changed), the top facesheet and the

top portion of the core pick up additional shear stress compared to the pristine case. In fact, at 27,746 cycles, the maximum shear stress in the core (denoted by triangle symbol in Figure 11) exceeds the core shear allowable (which has been reduced to 0.54 MPa after 27,746 cycles based on Basquin's Law. As the loading cycles on the beam continue, the bottom facesheet fails and, with its very low stiffness, it can support very little through-thickness shear stress. This then results in a large through-thickness shear stress gradient in the core and higher through-thickness shear stress in the top facesheet.

In Figure 10, the HyperMAC core failure prediction curve based on maximum shear stress is always (at least slightly) lower than the facesheet failure prediction curve, indicating that using the average core shear stress provides a more realistic failure prediction compared to experiment. However, these results may also indicate that, even when the facesheet failure mode is active, by the time the beam fails, the core may be close to failure and core damage may have even initiated.

The HyperMAC predictions for the fatigue life of the WF51 foam core beam are compared to experiment in Figure 12. In contrast to the H100 foam core beam data, the transition from core shear failure to facesheet failure is now well below the core static failure level (34.5 N/mm). The experimental data showed this transition between 16684 and 21073 cycles, whereas the HyperMAC model predicted the transition slightly higher at 26550 cycles. Clearly, the agreement between the model predictions and experiment is excellent.

Figure 13 compares the HyperMAC predictions with Basquin's Law predictions for the WF51 foam core beam. The HyperMAC and Basquin's Law predictions are again in close agreement for core failure. For facesheet failure, the curve predicted using Basquin's Law has a somewhat lower magnitude slope than does that predicted by HyperMAC. This is expected as the Basquin's Law characterization for the facesheet had a lower slope compared to the HyperMAC model characterization (except near the tail) as shown in Figure 4. As in the H100 foam core beam, the HyperMAC model for the core using the maximum core shear stress to predict damage initiation gives a lower predicted curve for core failure. In the region of the fatigue plot controlled by facesheet failure, the core max stress prediction again follows the facesheet failure curve closely and again predicts damage initiation in the core at slightly lower number of cycles than facesheet failure. As before, this indicates that the average core stress is a better indicator of core failure, although some core damage may initiate prior to facesheet failure.

As mentioned previously, the trace of the inverse of the beam's ABD matrix is tracked during the HyperMAC fatigue simulation to serve as a final failure criterion when it changes by an order of magnitude. This also serves as a measure of the beam's overall change in compliance due to damage as the cycles are applied. In

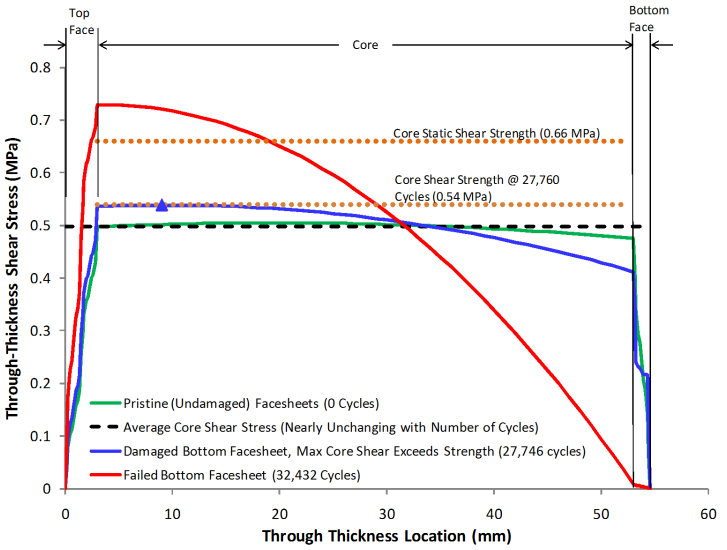

Figure 11: Example of the variation in the beam through-thickness shear stress distribution as fatigue damage progresses for the WF51 foam core beam.

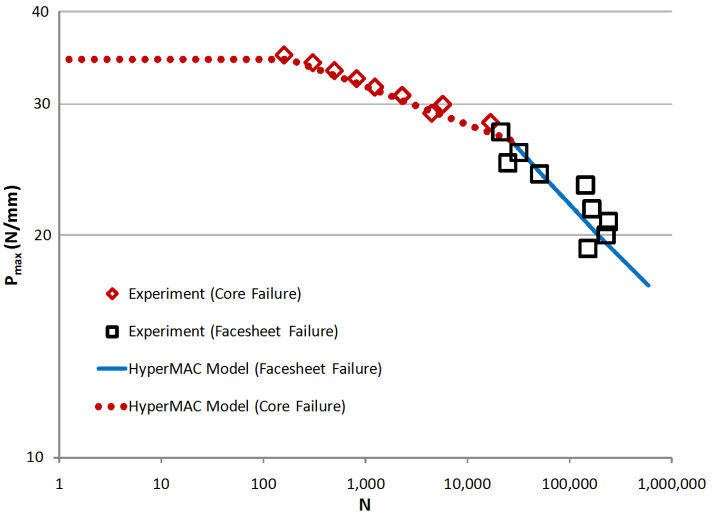

Figure 12: HyperMAC prediction of the fatigue life of the WF51 foam core beam tested in four point bending, along with experimental data [Zenkert and Burman (2011)].

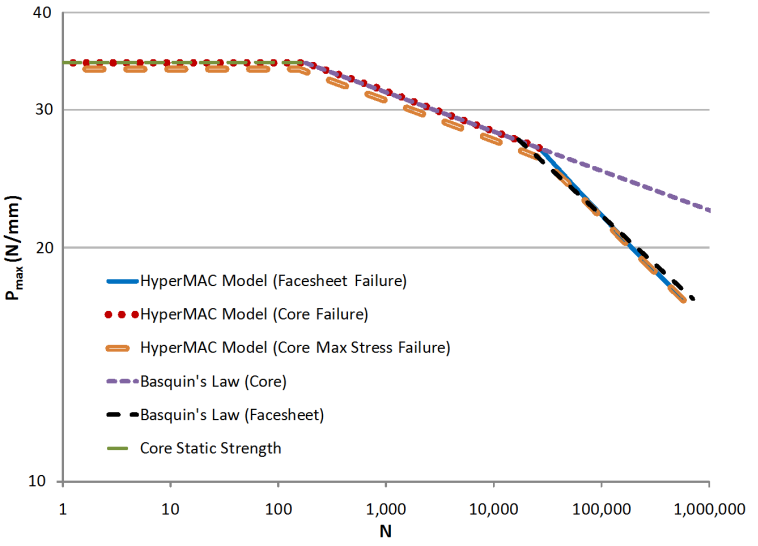

Figure 13: HyperMAC prediction of the fatigue life of the WF51 foam core beam tested in four point bending, compared with Basquin's Law predictions.

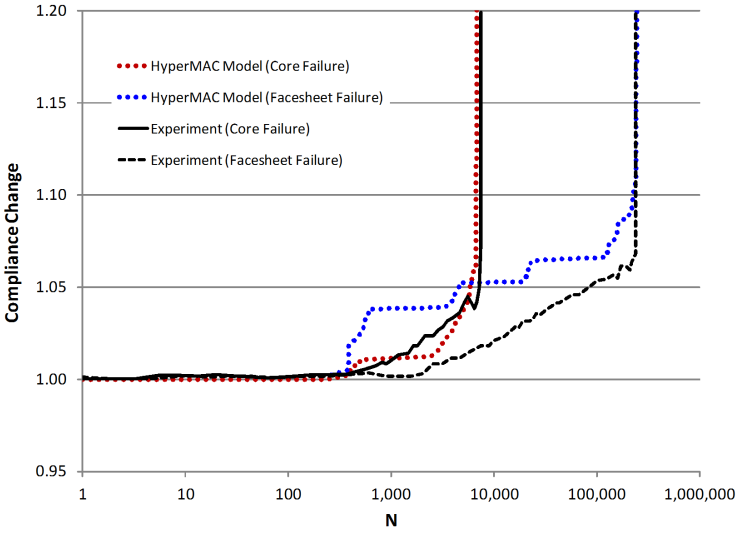

Figure 14: HyperMAC prediction of the WF51 foam core beam compliance change (trace of the inverse of the ABD matrix) compared to experimental data [Zenkert and Burman (2011)].

Figure 14, this value is plotted for the WF51 foam core beam for a case that failed due to core failure and a case that failed due to facesheet failure. These data are compared to experimental data given by Zenkert and Burman [Zenkert and Burman (2011)], wherein the beam's compliance for a given cycle was determined by determined by dividing the applied displacement range (maximum displacement minus minimum displacement) by the applied load range (maximum load minus minimum load). To obtain the compliance change, in both the simulation and experiment, the measure of compliance for a given cycle was divided by the compliance measure of the first cycle. The actual applied load levels for the experimental curves shown in Figure 14 were not given by Zenkert and Burman [Zenkert and Burman (2011)]. Thus, to select the appropriate applied load level to plot for comparison, the number of cycles at which the compliance change increased rapidly in the experimental data was matched as closely as possible with the number of cycles to failure in a simulation.

Despite the fact that the HyperMAC simulation considers only a single point along the beam (where the load is applied), it matches the measured compliance change history in the beam quite well. The agreement for the beam that failed due to core failure is excellent. For the beam that failed due to facesheet failure, the HyperMAC simulation overpredicts the compliance change somewhat, although it matches the initiation point quite well. Figure 14 clearly demonstrates that the HyperMAC fatigue simulation captures the primary characteristics of the four point bend sandwich beam behavior. Obviously, this type of information is not available from the phenomenological Basquin's Law approach.

As a final example, we consider the case in which the fiber volume fraction of the WF51 foam core beam has been varied from 42% to plus and minus 8%. In VARTM manufacturing, like that used to produce the foam core beams considered herein, some fiber volume fraction variability can be expected as this is controlled by the amount of infiltrated resin. Further, modeling changes in fiber volume fraction cannot be easily accommodated by the Basquin's Law approach on the scale of the laminate. Rather, new laminate level fatigue life test data, like that shown in Figure 4, would need to be generated in order to determine the new Basquin's Law parameters for each laminate with a different fiber volume fraction. Likewise, altering the laminate layup (e.g., adding a ply or altering the layup angles) would also require generation of new test data for the macro Basquin's Law approach, whereas, the present HyperMAC model can easily be altered to accommodate such changes. Note that, it would be possible to apply Basquin's Law at the ply level, but this would require, at a minimum, a generalization of Basquin's Law to handle the stark differences in the ply response in the fiber direction, transverse to the fiber direction, and in shear.

Figure 15 shows the effect of the significant changes in fiber volume fraction of the facesheets on the WF51 core beam fatigue life. As expected, increasing the fiber volume fraction extends the life at a given load level, while decreasing the fiber volume fraction decreases the life. The regions of the fatigue life curves controlled by core failure are unaffected, although the location of the transition of the failure mode is significantly affected by the facesheet fiber volume fraction. It is also interesting to note the relatively large scatter in the experimental data for facesheet failure (compare to Figure 9) is now bounded by the 34% and 50% facesheet fiber volume fraction cases. Hence, this or some other microstructural related variation (e.g., void content, fiber angle) could be responsible for the observed scatter. An approach that actually considers the microstructure is needed to examine such effects.

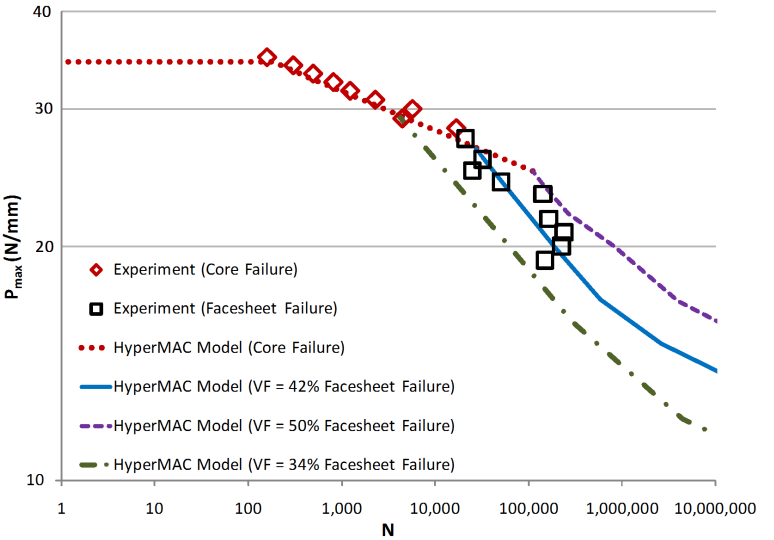

Figure 15: HyperMAC prediction of the fatigue life of the WF51 foam core beam tested in four point bending where the facesheet fiber volume fraction has been varied.

5 Conclusion

An important failure mode, cyclic fatigue failure, has been newly incorporated within the HyperSizer Composite Analysis and Structural Sizing Software. The capability predicts panel fatigue failure based on the accumulation of damage from the fiber/matrix constituent scale. Based on the constituent scale stress and strain

history for a given panel level load cycle, local damage is predicted, and the effects of this damage are homogenized to the ply, laminate, and panel levels. Global failure is then predicted based on the resultant loss of load carrying capability on the panel level. The micro scale calculations use NASA's Micromechanics Analysis Code with Generalized Method of Cells (MAC/GMC) software, which has been coupled with HyperSizer in a code called HyperMAC.

HyperMAC multiscale fatigue life predictions were made for E-glass/vinylester composite facesheet – foam core sandwich panels with two types of commercially available foam core materials and compared with experimental data from the literature [Zenkert and Burman (2011)]. Static and cyclic failure data were provided for the quasi-isotropic laminate facesheets and the core materials. Based on published stiffness and strength data for the E-glass fiber and the vinylester resin, HyperMAC predicted the static tensile strength of the facesheet laminate within 1.3% of the experimental value. For the fatigue life predictions, the fatigue life data for the quasi-isotropic laminate were used to back out the four required fatigue model parameters for the isotropic vinylester resin material. The foam core material was treated as homogeneous, with a shear strength that decreased as a function of cycles according to a Basquin's Law fit to the core experimental fatigue data.

The HyperMAC predictions agreed very well with experimental fatigue life data for two types of sandwich beams. For the WF51 core beam, which showed the clearer failure mode shift, compliance change data was also captured well by the HyperMAC model. In comparison to a completely phenomenological approach, wherein the facesheet fatigue response is modeled using a curve fit to the experimental facesheet fatigue data (e.g., using Basquin's Law), the HyperMAC approach captures the physics of the problem to a much greater extent. Further, once the resin material has been characterized, any microstructural changes can be easily accommodated without needing to re-test the facesheet laminate. The same is true for changes in the type of loading. Compared to a ply level approach, the HyperMAC methodology still has the advantage of progressing to a more fundamental scale, where damage actually occurs, and the associated ability to handle more types of microstructural variations. In addition, by capturing fatigue damage at the constituent scale, HyperMAC can utilize an isotropic fatigue model formulation for the constituents and then naturally predict the effects of damage at the ply scale. As the resin damages due to the cyclic loading, the differences in the behavior of the 0° and 90° plies is predicted by the physical arrangement of the damaged matrix. In contrast, at the ply level, a much more complex fatigue model would be needed, requiring characterization of significantly more parameters.

Acknowledgment

The second author gratefully acknowledges funding for this work provided by NASA's Aviation Safety Program Integrated Vehicle Health Management Project (Contract NNC07CN66C) with Dr. Steven M. Arnold as Technical Monitor. In addition, the authors acknowledge several helpful communications with Dan Zenkert of Kungliga Tekniska Högskolan, Stockholm, Sweden, regarding the experimental data presented herein.

References

Abbadi, A.; Azari, Z.; Belouettar, S.; Gilgert, J.; Freres, P. (2010): Modeling the Fatigue Behaviour of Composites Honeycomb Materials (Aluminium/Aramid Fibre Core) Using Four-Point Bending Tests. *International Journal of Fatigue*, vol. 32, pp. 1739-1747.

Aboudi, J. (2004): The Generalized Method of Cells and High-Fidelity Generalized Method of Cells Micromechanical Models—A Review. *Mechanics of Advanced Materials and Structures*, vol. 11, pp.329-366.

Aboudi, J.; Arnold, S.M.; Bednarcyk, B.A. (2013): *Micromechanics of Composite Materials a Generalized Multiscale Analysis Approach*, Elsevier, New York.

Arnold, S.M.; Kruch, S. (1991): Differential Continuum Damage Mechanics Models for Creep and Fatigue of Unidirectional Metal Matrix Composites. NASA TM 105213.

Arnold, S.M.; Kruch, S. (1994): Differential Continuum Damage Mechanics Models for Creep and Fatigue of Unidirectional Metal Matrix Composites. *International Journal of Damage Mechanics*, vol. 3, pp. 170-191.

Bednarcyk, B.A.; Arnold, S.M. (2002): MAC/GMC 4.0 User's Manual Volume 2: Keywords Manua. NASA/TM-2002-212077/Vol 2.

Bednarcyk, B.A.; Yarrington, P.W.; Collier, C.S.; Arnold, S.M. (2006): Progressive Failure Analysis of Composite Stiffened Panels, in *Proc. 47th AIAA/ASME/ASCE/AHS/ASC Structures, Structural Dynamics, and Materials Conference*, May, Newport, Rhode Island, AIAA-2006-1643.

Bednarcyk, B.A.; Aboudi, J.; Yarrington, P.W. (2007): Determination of the Shear Stress Distribution in a Laminate From the Applied Shear Resultant—A Simplified Shear Solution. NASA/TM-2007-215022.

Bednarcyk, B.A.; Arnold, S.M. (2010): Aboudi's Micromechanics Theories Applied to Multiscale Analysis of Composites. *Advances in Mathematical Modeling and Experimental Methods for Materials and Structures. The Jacob Aboudi Volume*, Springer, New York.

Burman, M.; Zenkert, D. (1997): Fatigue of Foam Core Sandwich Beams – 1: Undamaged Specimens. *International Journal of Fatigue*, vol. 19, pp. 551–561.

Burman, M.; Zenkert, D. (1997): Fatigue of Foam Core Sandwich Beams – 2: Effect of Initial Damage. *International Journal of Fatigue*, vol. 19, pp.563–578.

Camata, G.; Shing, P.B. (2010): Static and Fatigue Load Performance of a GFRP Honeycomb Bridge Deck. *Composites: Part B*, vol. 41, pp. 299-307.

Chrupalla, D.; Kreikemeier, J.; Berg S.; Kärger, L.; Dorielle, M.; Ludwig, T.; Jansen, E.; Rolfes, R.; Kling, A. (2012): A Loose Coupling Multiscale Approach for the Detailed Analysis of the Influence of Critical Areas on the Global Behaviour of Composite Structures. *CMC: Computers, Materials & Continua*, vol. 32, pp.159-176.

Collier Research Corp. (2013): HyperSizer Composite Analysis and Structural Sizing Software, http://www.hypersizer.com.

Dai, J.; Hahn, H.T. (2004): Fatigue Analysis of Sandwich Beams using a Wear-out Model. *Journal of Composite Materials*, vol. 38, pp. 581–589.

Dong, L.; Atluri, S.N. (2013): SGBEM Voronoi Cells (SVCs), with Embedded Arbitrary-Shaped Inclusions, Voids, and/or Cracks, for Micromechanical Modeling of Heterogeneous Materials. *CMC: Computers, Materials & Continua*, vol. 33, pp.111-154.

DIAB AB (2011): *Divinycell H Technical Manual*, http://www.diabgroup.com/italy/literature/i_pdf_files/man_pdf/ H_man.pdf.

Devold AMT (2011): http://www.amt.no/?menu=50&id=39.

El Mahi, A.; Farooq, M.K.; Sahraoui, S.; Bezazi, A. (2004): Modeling the Flexural Behavior of Sandwich Composite Materials under Cyclic Fatigue. *Materials and Design*, vol. 25, pp. 199–208.

Evonik Industries (2011): http://www.rohacell.com/sites/dc/Downloadcenter/Evonik/Product/ROHACELL/product- information/ROHACELL%20WF%20Product%20Information.pdf.

Feyel, F. (1999): Multiscale FE^2 Elastoviscoplastic Analysis of Composite Structures. *Computational Materials Science*, vol. 16, pp.344-354.

Jen, Y.M.; Chang, L.Y. (2008): Evaluating Bending Fatigue Strength of Aluminum Honeycomb Sandwich Beams Using Local Parameters. *International Journal of Fatigue*, vol. 30, pp. 1103-1114.

Jen, Y.M.; Chang, L.Y. (2009): Effect of Amount of Adhesive the Bending Fatigue Strength of Adhesively Bonded Aluminum Honeycomb Sandwich Beams. *International Journal of Fatigue*, vol. 31, pp. 455-462.

Jen, Y.M.; Chang, L.Y. (2009): Effect of Thickness of Face Sheet on the Bending Fatigue Strength of Aluminum Honeycomb Sandwich Beams. *Engineering Failure Analysis*, vol. 16, pp. 1282-1293.

Kanny, K.; Mahfuz, H. (2005): Flexural Fatigue Characteristics of Sandwich Structures at Different Loading Frequencies. *Composite Structures*, vol. 67, pp. 403–410.

Naghipour, P.; Pineda, E.J.; Arnold, S.M. (2013): A Novel Approach to Modeling of Interfacial Fiber/Matrix Cyclic Debonding. *CMC: Computers, Materials & Continua*, In Press.

Reichhold, Inc. (2011): http://www.reichhold.com/documents/910_DION9500U-S.pdf.

Sharma, N.; Gibson, R.F.; Ayorinde, E.O. (2006): Fatigue of Foam and Honeycomb Core Composite Sandwich Structures: A Tutorial. *Journal of Sandwich Structures and Materials*, vol. 8, pp. 263-319.

Soden, P.D.; Hinton, M.J.; Kaddour, A.S. (1998): Properties, Lay-Up Configuration and Loading Conditions for a Range of Fibre-Reinforced Composite Laminates. *Composites Science and Technology*, vol. 58, pp. 1011-1022.

Wilt, T.E.; Arnold, S.M.; Saleeb, A.F. (1997): A Coupled/Uncoupled Computational Scheme for Deformation and Fatigue Damage Analysis of Unidirectional Metal-Matrix Composites. *Applications of Continuum Damage Mechanics to Fatigue and Fracture*, ASTM STP 1315, D.L. McDowell (Ed.), 65-82.

Xiang, Y.; Liu, Y. (2010): Inverse FORM Method for Probabilistic Fatigue Prognosis, in *Proc. 51st AIAA/ASME/ASCE/AHS/ASC Structures, Structural Dynamics, and Materials Conference*, April, Orlando, Florida, AIAA 2010-2684.

Xiang, Y.; Liu, Y. (2011): An Equivalent Stress Level Model for Efficient Fatigue Crack Growth Prediction, in *Proc. 52nd AIAA/ASME/ASCE/AHS/ASC Structures, Structural Dynamics, and Materials Conference*, April, Denver, Colorado, AIAA 2011-2033.

Zenkert, D.; Burman, M. (2011): Failure Mode Shifts During Constant Amplitude Fatigue Loading of GFRP/Foam Core Sandwich Panels. *International Journal of Fatigue*, vol. 33, pp. 217-222.

Zenkert, D. (2011): Personal Communication.